

Microscale Simulation of Martensitic Microstructure Evolution

Valery I. Levitas,¹ Alexander V. Idesman,¹ and Dean L. Preston²

¹Center for Mechanochemistry and Synthesis of New Materials, Department of Mechanical Engineering, Texas Tech University, Lubbock, Texas 79409-1021, USA

²Physics Division, Los Alamos National Laboratory, Los Alamos, New Mexico 87545, USA

(Received 9 December 2003; published 3 September 2004)

A new model for the evolution of multivariant martensitic microstructure in single crystals and polycrystals is developed. In contrast with Landau-Ginzburg models, which are limited in practice to nanoscale specimens, this new scale-free model is valid for length scales greater than 100 nm and without an upper bound. It is based on a thermodynamic potential in the volume fractions of the martensitic variants that exhibits an instability resulting in microstructure formation. Simulated microstructures in elastic single crystals and polycrystals under uniaxial loading are in qualitative agreement with those observed experimentally.

DOI: 10.1103/PhysRevLett.93.105701

PACS numbers: 64.70.Kb, 64.60.-i, 81.30.Kf

The martensitic microstructure (MM) that is formed, e.g., in a steel or a shape memory alloy (SMA) as a result of a martensitic phase transformation (PT), determines the physical and deformation properties of the material, internal stresses, and possible engineering applications. The evolution of MM has been investigated using the phase field approach [1] in which multiple diffuse interfaces between austenite, A , and the m martensitic variants, M_i , appear as solutions of evolution equations for the order parameters. The main problem is that for PT in steel and SMA the widths of the interfaces between the M_i and between A and M_i are ~ 1 nm. Resolution of the order parameter variation requires at least three grid cells; thus only single nanocrystals or polynanocrystals can be treated, while the grain sizes in typical engineering materials are 10–1000 μm . Previous microscale approaches [2,3] determine only the continuous distribution of volume fraction of martensitic variants but not the discrete MM.

A typical martensitic unit consists of alternating planar slabs of two M_i , often twin related. Since the slab thickness is $d \simeq 10$ nm, it is impractical to model each of the thousands of layers in a mm-sized sample. In this Letter we develop a new model for the evolution of MM in single crystals and polycrystals by averaging over microstructures at length scales of $l \simeq 10d \simeq 100$ nm. This coarse-graining procedure is based on a representative microscale volume element of size l comprised of A and M ; M itself consists of multiple alternating thin layers of two variants M_1 and M_2 , which could be any two of the m possible variants, divided by parallel plane interfaces. Since there are no interface widths greater than 100 nm, the gradient energy is dropped, which removes the only length scale from the theory. Thus, our model is scale invariant and any system larger than 100 nm can be treated. The volume fractions \bar{c}_i of the M_i are the order parameters. Our microscale potential $G(\bar{c}_i, \dots)$ accounts for internal stresses between A and

M and between M_1 and M_2 that are determined explicitly using anisotropic elasticity. This results in a characteristic instability region in the local (microscopic) stress-strain curve (Fig. 1). Finite-element simulations based on the developed model exhibit the formation of MM similar to that observed experimentally.

Thermomechanical model.—The transformation (Bain) strain ϵ_{ii} transforms the crystal lattice of A into the lattice of M_i . Consider a macroscopic single or polycrystalline sample in which the MM is determined by solution of a boundary-value problem. Each material point of the sample is a microscale volume element comprised of A and M (volume fraction c) divided by a planar interface. The M itself consists of large numbers of alternating thin layers of two variants, M_1 and M_2 , divided by parallel plane interfaces, with volume fractions c_1 and $c_2 = 1 - c_1$ with respect to M . The volume fraction of M_i in the $A + M$ mixture is $\bar{c}_i = cc_i$; $\bar{c}_1 + \bar{c}_2 = c$.

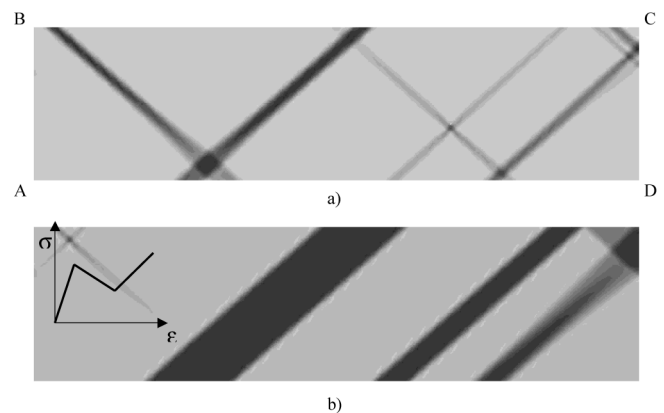


FIG. 1. Distribution of the volume fraction of M_1 at two different macrostrains (a) $\epsilon = 0.015\%$ and (b) $\epsilon = 0.05\%$ for five initial nuclei. The black (white) regions correspond to $\bar{c}_1 = 1$ ($\bar{c}_1 = 0$). The inset shows a local microscopic stress-strain diagram with an instability region.

We assume additive decomposition of the total strain $\boldsymbol{\varepsilon}$ into elastic, $\boldsymbol{\varepsilon}_e$, and transformational, $\boldsymbol{\varepsilon}_t$, parts

$$\boldsymbol{\varepsilon} = \boldsymbol{\varepsilon}_e + \boldsymbol{\varepsilon}_t, \quad \boldsymbol{\varepsilon}_t = c \sum_{i=1}^2 \boldsymbol{\varepsilon}_{ti} c_i. \quad (1)$$

The Gibbs potential for the representative microscale volume element is

$$\begin{aligned} G(\boldsymbol{\sigma}, \bar{c}_i, \theta) &= G_e(\boldsymbol{\sigma}, \bar{c}_i, \theta) - \boldsymbol{\sigma} : \boldsymbol{\varepsilon}_t + (1 - c) G_A^\theta(\theta) \\ &\quad + c G_M^\theta(\theta) + G_{\text{in}}(\bar{c}_i), \\ G_{\text{in}} &= c B_{12} c_1 c_2 + B c (1 - c) \geq 0. \end{aligned} \quad (2)$$

Here G_e is the elastic part of the Gibbs potential, G_A^θ and G_M^θ are the thermal energies of A and M , θ is the temperature, G_{in} is the energy of internal stresses due to the elastic interactions between the variants M_1 - M_2 (first term) and between A and M (second term), $\boldsymbol{\sigma}$ is the stress, $\boldsymbol{\sigma} : \boldsymbol{\varepsilon}_t = \sigma_{ij} \varepsilon_t^{ji}$ is the transformation work, and B and B_{12} are parameters.

The first term in G_{in} was derived by solving the elasticity problem for a layered alternating M_1 - M_2 structure under zero external stresses. Let the 3-axis of the local orthogonal coordinate system be normal to the M_1 - M_2 interface. We divide the six components of the stress tensor into two vectors: $\boldsymbol{\sigma}^\perp = (\sigma_{13}, \sigma_{23}, \sigma_{33})$, which contains the components normal to the M_1 - M_2 interface, and $\boldsymbol{\sigma}^\parallel = (\sigma_{11}, \sigma_{12}, \sigma_{22})$, which contains the in-layer components of the stress; the same is done for $\boldsymbol{\varepsilon}$ and $\boldsymbol{\varepsilon}_t$. Then Hooke's law for each layer is

$$\begin{pmatrix} \boldsymbol{\sigma}_i^\parallel \\ \boldsymbol{\sigma}_i^\perp \end{pmatrix} = \begin{pmatrix} \mathbf{E}_\parallel & \mathbf{E}_\square \\ \mathbf{E}_\square & \mathbf{E}_\perp \end{pmatrix} \begin{pmatrix} \boldsymbol{\varepsilon}_i^\parallel - \boldsymbol{\varepsilon}_{ii}^\parallel \\ \boldsymbol{\varepsilon}_i^\perp - \boldsymbol{\varepsilon}_{ii}^\perp \end{pmatrix}, \quad (3)$$

where \mathbf{E}_\parallel , \mathbf{E}_\perp , and \mathbf{E}_\square are the corresponding matrix parts of the elasticity tensor. [The problem was also solved for phases with different elastic properties, but the result does not have the simple structure of Eq. (2).] The homogeneous stress and strain in each phase satisfy the equilibrium and compatibility equations. Continuity of normal stresses and tangential displacements across the interface, and zero averaged (external) stress result in $\boldsymbol{\sigma}_1^\perp = \boldsymbol{\sigma}_2^\perp = 0$, $\boldsymbol{\varepsilon}_1^\parallel = \boldsymbol{\varepsilon}_2^\parallel$, and $c_1 \boldsymbol{\sigma}_1^\parallel + c_2 \boldsymbol{\sigma}_2^\parallel = 0$. Solving the above equations, we obtain for each layer

$$\boldsymbol{\varepsilon}_i^\perp - \boldsymbol{\varepsilon}_{ii}^\perp = c_j \mathbf{E}_\perp^{-1} \mathbf{E}_\square \Delta \boldsymbol{\varepsilon}_t; \quad \boldsymbol{\varepsilon}_i^\parallel - \boldsymbol{\varepsilon}_{ii}^\parallel = -c_j \Delta \boldsymbol{\varepsilon}_t, \quad (4)$$

where $\Delta \boldsymbol{\varepsilon}_t = \boldsymbol{\varepsilon}_{t1}^\parallel - \boldsymbol{\varepsilon}_{t2}^\parallel$; here and later $i, j = 1, 2$, $j \neq i$. Substituting Eq. (4) into Eq. (3), we obtain the stresses and then calculate the energy of each layer G_i . After averaging the energy of internal stresses over the martensite, one obtains $G_{\text{in}} = c_1 G_1 + c_2 G_2 = B_{12} c_1 c_2$ with $B_{12} = \Delta \boldsymbol{\varepsilon}_t (\mathbf{E}_\parallel - \mathbf{E}_\square \mathbf{E}_\perp^{-1} \mathbf{E}_\square) \Delta \boldsymbol{\varepsilon}_t / 2 \geq 0$.

As expected, the internal stresses of the layered martensite are due to the discontinuity $\Delta \boldsymbol{\varepsilon}_t$ in the in-layer components of the transformation strain across the inter-

faces. The discontinuity depends on the orientation of the interface with respect to the crystal lattice and can be computed by rotating $\boldsymbol{\varepsilon}_{t1} - \boldsymbol{\varepsilon}_{t2}$ to the local coordinates normal and parallel to the layers. The actual orientation of the M_1 - M_2 interface is determined by minimization of B_{12} and therefore G , which can be done before solution of the boundary-value problem for MM formation. If $\Delta \boldsymbol{\varepsilon}_t = 0$ for some interface orientation, then $B_{12} = 0$, which is the case for twin-related variants and is studied in the crystallographic theory of M [4].

The second term in G_{in} , which represents the energy of the elastic interactions between A and M , was derived by following the same approach as for the first term under the assumption of stress and strain homogeneity in A and an averaged M mixture. We find $B = \boldsymbol{\varepsilon}_{Mt}^\parallel (\mathbf{E}_\parallel - \mathbf{E}_\square \mathbf{E}_\perp^{-1} \mathbf{E}_\square) \boldsymbol{\varepsilon}_{Mt}^\parallel / 2 \geq 0$ with $\boldsymbol{\varepsilon}_{Mt} = \boldsymbol{\varepsilon}_t / c$. Note that our results for B_{12} and B are in agreement with general estimates for G_{in} in [4,5]. However, unlike the $M_1 - M_2$ case, the orientation of the $A - M$ interface is determined as part of the solution of a boundary-value problem for MM formation. After an initial transitional stage during which $A - M$ interfaces are not defined, $c = 0$ or $c = 1$ almost everywhere (see Figs. 1-3); i.e., sharp interfaces form, and the B term vanishes except on the interfaces. Even if $\boldsymbol{\varepsilon}_{Mt}^\parallel$ can be made to vanish, e.g., as in the stress-free crystallographic theory of MM [4], we need to use $B > 0$ because (i) the solutions of boundary-value problems exhibit curved and irregular interfaces and deviation of plane interfaces from the invariant plane (see Fig. 3 and discussion below), i.e., $\boldsymbol{\varepsilon}_{Mt}^\parallel \neq 0$, and (ii) additional elastic energy is concentrated at $A - (M_1 + M_2)$ interfaces due to the finite width of M_i and incompatibility of each M_i and A . Since B affects the driving force for the $A - M$ PT [Eq. (5)] and the macroscopic stress-strain (σ - ε) curve, it can be determined by comparing experimental and computational macroscopic σ - ε curves. We use $B = \text{const} > 0$ for the simulation results presented below.

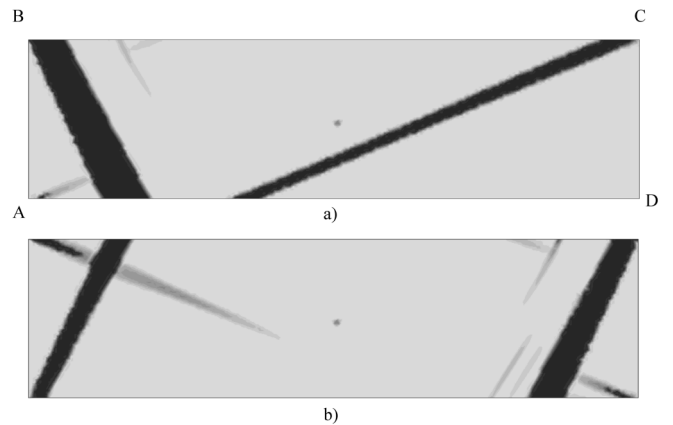


FIG. 2. Distribution of martensite at the macrostrain $\varepsilon = 0.1\%$ for two orientations of the crystal axes relative to the tensile direction: (a) \bar{c}_1 for $\beta = 30^\circ$; (b) \bar{c}_2 for $\beta = 60^\circ$.

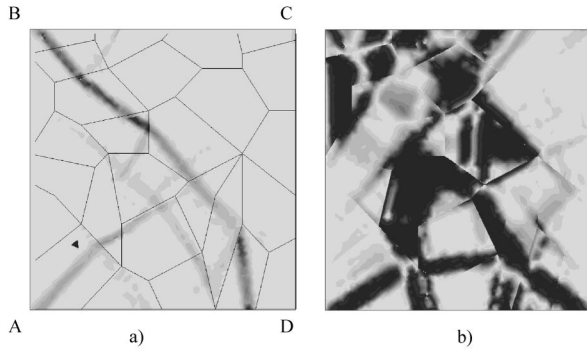


FIG. 3. Distribution of the volume fraction of martensite in a polycrystal at two different macrostrains: (a) $\varepsilon = 0.02\%$; (b) $\varepsilon = 0.1\%$.

The only minima of G with respect to c on the interval $0 \leq c \leq 1$ are at $c = 0$ or $c = 1$ or both for all $\boldsymbol{\sigma}$, θ , and c_i ; thus the system is expected to tend to either pure M ($c = 1$) or pure A ($c = 0$) at each material point, i.e., to a discrete $A - M$ microstructure. Neglecting terms in G_e higher than linear in c , this condition requires $B > 0$, which is consistent with $G_{in} \geq 0$.

The dissipation rate due to the PT is $D = -\dot{G} - \dot{\boldsymbol{\sigma}}:\boldsymbol{\varepsilon} - s\dot{\theta} \geq 0$, where s is the entropy. Inserting (2) into it, making use of (1), and accounting for the independence of D of $\dot{\boldsymbol{\sigma}}$ and $\dot{\theta}$, we obtain the elasticity relation $\boldsymbol{\varepsilon}_e = -\partial G_e / \partial \boldsymbol{\sigma}$, the entropy $s = -\partial G / \partial \theta$, and the residual dissipative inequality $D = \sum_{i=1}^2 X_i \dot{c}_i = \sum_{i=1}^2 X_{i0} \dot{c}_{i0} + X_{21} \dot{c}_{21} \geq 0$;

$$X_{i0} = -\frac{\partial G}{\partial \bar{c}_i} = \boldsymbol{\sigma}:\boldsymbol{\varepsilon}_{ii} - \frac{\partial G_e}{\partial \bar{c}_i} - \Delta G^\theta - B(1 - 2c) - B_{12}c_2^2. \quad (5)$$

Here X_{i0} is the driving force for the $A \rightarrow M_i$ PT, $X_{21} = X_{20} - X_{10} = \boldsymbol{\sigma}:(\boldsymbol{\varepsilon}_{i2} - \boldsymbol{\varepsilon}_{i1}) - B_{12}(1 - 2c_2)$ is the driving force for the $M_1 \rightarrow M_2$ PT, $\Delta G^\theta = G_M^\theta - G_A^\theta$, \dot{c}_{ij} is the rate of change of c_i due to a PT from the phase j to i , $\dot{c}_{ij} = -\dot{c}_{ji}$, and $\dot{c}_i = \sum_{j=0}^2 \dot{c}_{ij}$. The following PT criteria and kinetic equations for the \dot{c}_{ij} are used:

$$\begin{aligned} |X_{ij}| > k_{ij} &\Rightarrow \dot{c}_{ij} = \lambda_{ij} \text{sgn} X_{ij} (|X_{ij}| - k_{ij}); \\ |X_{ij}| \leq k_{ij} &\Rightarrow \dot{c}_{ij} = 0. \end{aligned} \quad (6)$$

Here $k_{ij} = k_{ji}$ is the given critical value of the driving force for the $i \rightarrow j$ PT due to interface friction and $\lambda_{ij} = \lambda_{ji}$ are kinetic coefficients. Surface energy can be effectively included in k_{ij} . In contrast to microscale models [2,3], we put $k_{0j} = k_{j0} = 0$ if $c_i(1 - c) \neq 0$; i.e., after satisfying the $0 \leftrightarrow i$ PT criteria at $c = 1$ or $c_i = 0$ there is no barrier for the $0 \leftrightarrow i$ PT. Otherwise the system can be arrested at some intermediate c . Alternatively, we can put $k_{0j} = 0$ and effectively include the actual value $k = k_{0j}$ in B . Among the m possible variants, we choose the first two variants that satisfy the PT criterion (6).

Numerical modeling.—The developed model was incorporated in the finite-element code ABAQUS [6] with six-node quadratic triangular elements. We simulated the formation of MM due to a cubic-tetragonal PT in a plane-strained specimen under uniaxial tension. Two twin-related variants were considered: $\boldsymbol{\varepsilon}_{t1} = -\boldsymbol{\varepsilon}_{t2}$ with components $(\boldsymbol{\varepsilon}_{t1})_{11} = -(\boldsymbol{\varepsilon}_{t1})_{22} = 0.1$ and $(\boldsymbol{\varepsilon}_{t1})_{12} = 0$. Since the M_i are twin related, $B_{12} = 0$. We assume for simplicity that $G_e = -\boldsymbol{\sigma}:\mathbf{S}:\boldsymbol{\sigma}/2$, where \mathbf{S} is the fourth-order isotropic compliance tensor, the same for A and M . This implies Hooke's law, $\boldsymbol{\varepsilon}_e = \mathbf{S}:\boldsymbol{\sigma}$, and $X_{i0} = \boldsymbol{\sigma}:\boldsymbol{\varepsilon}_{ii} - \Delta G^\theta - B(1 - 2c)$. The condition $X_{i0} = 0$ gives an equilibrium stress-strain curve with a decreasing (unstable) region (Fig. 1); such an instability (realized only for $B > 0$) is a necessary condition for strain localization and the formation of a MM. The following material parameters were used: Young modulus $E = 2 \cdot 10^5$, $B = 0.1$, $k_{10} = k_{20} = 0.2$, $k_{21} = 0$ (all in MPa), Poisson ratio $\nu = 0.3$, $\lambda_{10} = \lambda_{20} = \lambda_{21} = 10 \text{ MPa}^{-1} \text{ s}^{-1}$, and $\Delta G^\theta = 0$. The boundary conditions on the rectangular specimen are as follows: AB is fixed, CD moves at a constant normal velocity corresponding to the macrostrain rate $\dot{\varepsilon} = 5 \times 10^{-9} \text{ s}^{-1}$, and BC and AD are stress-free. The initial state is stress-free A except for small single or multiple M nuclei ($\bar{c}_1 = 1$). The mesh and time step independence of the solutions was verified.

In the problem shown in Fig. 1, which was solved with 6614 elements and 13487 nodes, $\bar{c}_2 \approx 0$. The PT initiates at five initial M_1 nuclei, each a single finite element. A pair of thin orthogonal plates forms around each nucleus at 45° to the tension axis. The plates in each pair initially grow at the same rate, but eventually some of the plates begin to shrink while others continue to grow; three plates survive [Fig. 1(b)]. Thus a reverse PT occurs in some regions under monotonic loading. This phenomenon is quite unexpected and is not predicted by other MM-free micromechanical models [2,3]. All plates are parallel to the invariant plane for $\boldsymbol{\varepsilon}_{t1}$. Similar results were obtained for a single initial nucleus.

Figure 2 shows the MM for a crystal lattice rotated with respect to the tensile direction by angles $\beta = 30^\circ$ [Fig. 2(a)] and $\beta = 60^\circ$ [Fig. 2(b)]. As in Fig. 1, only one martensitic variant predominates under increased loading: M_1 for $\beta = 30^\circ$ and M_2 for $\beta = 60^\circ$. Note that the M nucleus in the center of the specimen does not spawn any M plates, but instead the plates form near the corners as a result of stress concentration.

All obtained results, namely, the formation of single or multiple M plates parallel to the invariant plane, nucleation in regions of stress concentration or at free surfaces, oscillations in the macroscopic stress-strain curve, and a strong dependence of microstructure on crystal orientation, are observed in numerous experiments [7,8].

Figure 3 exhibits the formation of MM in an untextured (random grain orientations) polycrystal. The initial state is A ($c = 0$) with two small M_1 nuclei, one of which does not induce a PT. The mesh consists of 2478 elements with

5091 nodes. During the initial stages of the PT, the growing M plates propagate from one grain to another. Three plates are formed that cross at least half of the specimen, and all are oriented $\approx 45^\circ$ to the tension axis except in one grain where the plate is nearly orthogonal to the load. When the advancing plates cross grain boundaries the M can change from one variant to the other depending on the relative grain orientations and internal stress distribution; thus most of the plates consist of both variants. Essentially none of the plates formed during the initial stages of the PT are present in the final calculated state [Fig. 3(b)]. The calculated MM in Fig. 3 is in qualitative agreement with experimentally observed M microstructures in polycrystals (see, e.g., [9]): the MM is comprised of straight, curved, and irregular $A - M$ interfaces, small regions of residual A locked between M regions, and most of the M regions consist of both variants. Some plates significantly deviate from the invariant plane because of internal stresses and because the ratio c_1/c_2 depends on stress, which is in direct contrast to the invariant-plane variant derived in crystallographic theory and used in all micromechanical modeling [2].

Concluding remarks.—Unlike known phase field models [1,10], our microscale model (i) is based on a much larger representative volume element and tracks only the interfaces between A and mixtures of the M_i but does not track interfaces between the M_i , (ii) is scale invariant. The gradient (interface) energy, which is important at the nanoscale but not at the microscale, is dropped; this removes the only length scale from the theory and eliminates any upper bound on the system size, (iii) accounts for the experimentally observed features of martensitic PT in SMA and steels, specifically, constant (stress-independent) transformation strain tensor and stress hysteresis, and transformation at nonzero elastic moduli, and it can incorporate all temperature-dependent thermomechanical properties of both phases. As shown in [10], this is not the case for the nanoscale potentials in [1]. The nanoscale potential in [10] respects the above features, but it has not yet been used for numerical simulations of MM, and (iv) includes dissipative thresholds k_{ij} .

In contrast to known microscopic thermomechanical models [2,3], our microscale model (i) describes a discrete MM rather than a smeared distribution of A and M , (ii) is based on Bain strain variants rather than habit plane variants. The habit plane variant is a combination of two Bain strain variants in a specific fixed proportion independent of stress. It is known, however, that the ratio c_1/c_2 varies significantly with the applied stress. This is neglected in [2] but is taken into account in our theory and confirmed in simulations, (iii) is applicable at spatial scales down to 100 nm rather than 1–10 μm because the size of the representative volume element for Bain strain variants is smaller than that for habit plane variants, (iv) was obtained by a coarse-graining procedure based on a

representative volume element with simple geometry. Our parameters B and B_{12} were determined explicitly, whereas the parameters B and B_{ij} in [2] depend on the complex, unknown geometry of the M in the representative volume element and therefore can only be estimated, and (v) allows a much more accurate determination of the macroscopic mechanical properties, in particular, the macroscopic stress-strain curve, since they are sensitive to the geometry of the phases.

Our microscale model can be extended to encompass plastic materials by including single-crystal viscoplastic constitutive equations. Note that a stress-strain curve of the type shown in Fig. 1 leads to strain localization in macroscopic polycrystalline plasticity theory [8]. Incorporation of such a σ - ϵ curve for single crystals into our approach would enable us to describe the interaction between plastic and transformational instabilities, in particular, PT in shear bands and shear-band intersections, and to determine the conditions for slip or twinning as an accommodation mechanism. The use of such a curve in our macroscopic polycrystalline model for PT [3] would allow us to describe the MM at larger scales, as is observed in experiments on polycrystals [8].

LANL (52844) and TTU support for V. I. L. and A. V. I., and NSF funding (CMS-02011108) for V. I. L. are gratefully acknowledged. The technical assistance of J.-Y. Cho is appreciated.

-
- [1] Y.U. Wang *et al.*, *Acta Mater.* **49**, 1847 (2001); K. Rasmussen *et al.*, *Phys. Rev. Lett.* **87**, 055704 (2001).
 - [2] J. G. Boyd and D.C. Lagoudas, *Int. J. Plast.* **12**, 805 (1996); X. Gao, M. Huang, and L. C. Brinson, *Int. J. Plast.* **16**, 1345 (2000); T. J. Lim and D. L. McDowell, *J. Mech. Phys. Solids* **50**, 651 (2002).
 - [3] V.I. Levitas *et al.*, *J. Intell. Mater. Syst. Struct.* **9**, 324 (1998); **10**, 983 (1999).
 - [4] K. Bhattacharya, *Microstructure of Martensite. Why It Forms and How It Gives Rise to the Shape-Memory Effect* (Oxford University Press, New York, 2004).
 - [5] R.V. Kohn, *Continuum Mech. Thermodyn.* **3**, 193 (1991); K. Bhattacharya, *Continuum Mech. Thermodyn.* **5**, 205 (1993).
 - [6] ABAQUS, Hibbit, Karlsson and Sorensen Inc., Ver. 6.2, 2001.
 - [7] T. W. Shield, *J. Mech. Phys. Solids* **43**, 869 (1995).
 - [8] J. A. Shaw, *Int. J. Plast.* **16**, 541 (2000); Z. Q. Li and Q. P. Sun, *Int. J. Plast.* **18**, 1481 (2002).
 - [9] P.G. McDougall and C.M. Wayman, *The Crystallography and Morphology of Ferrous Martensite*, Martensite, edited by G. B. Olson and W. S. Owen (ASM International, Materials Park, OH, 1992), Chap. 5, pp. 59–95.
 - [10] V.I. Levitas and D.L. Preston, *Phys. Rev. B* **66**, 134206 (2002); V.I. Levitas, D. L. Preston, and D.-W. Lee, *Phys. Rev. B* **68**, 134201 (2003).